0270-6474/85/0508-2225$02.00/0

The Journal of Neuroscience
Vol. 5, No. 8, pp. 2225-2239
August 1985

Membrane Physiology of Retinal Glial (Müller) Cells[1]

ERIC A. NEWMAN

Eye Research Institute of Retina Foundation, Boston, Massachusetts 02114

Abstract

Electrophysiological techniques were used to determine the ion selectivity properties and the spatial distribution of the membrane conductance of amphibian Müller cells. Membrane potential changes recorded during ion substitution experiments in frog (*Rana pipiens*) retinal slices demonstrated that the Müller cell K^+:Na^+ membrane permeability ratio is approximately 490:1 and that cell Cl^- permeability is extremely low. In frog retinal slices, Müller cell input resistance was 8.5 megohms when measured in the inner plexiform layer and 4.8 megohms when measured in the optic fiber layer. Intact, enzymatically dissociated salamander (*Ambystoma tigrinum*) cells had an input resistance of 7.9 megohms, whereas cells lacking their endfoot process (removed by surgical microdissection or by shearing force) had a resistance of 152 megohms. Pressure ejection of a 100 mM K^+ solution near the proximal surface of the endfeet of dissociated salamander cells produced depolarizations 7 times greater than did ejections near the lateral face of the endfoot and 24 to 50 times greater than did ejections near other cell regions. Similar K^+ ejection results were obtained from Müller cells in salamander and frog retinal slices. Taken together, these results demonstrate that in both the frog and the salamander, approximately 95% of the total membrane conductance of Müller cells is localized in the cell's endfoot process. In salamander, the specific membrane resistance of the endfoot membrane was estimated to be 32 ohm·cm^2 whereas the specific resistance of the remainder of the cell was 7300 ohm·cm^2. This remarkably nonuniform conductance distribution has important consequences for theories concerning K^+ regulation in the retina and for mechanisms underlying electroretinogram generation.

The physiological properties of glial cell membrane were first studied by Stephen Kuffler and his colleagues 20 years ago. These investigators demonstrated that the membrane of both vertebrate and invertebrate glia is selectively permeable to potassium and is electrically inexcitable (Kuffler, 1967). Many types of glial cells have been shown to be almost exclusively permeable to K^+. These include glia of the vertebrate optic nerve (Kuffler et al., 1966), the spinal cord (Lothman and Somjen, 1975), the leech central nervous system (Kuffler and Potter, 1964; Nicholls and Kuffler, 1964), and astrocytes (Walz et al., 1984) and oligodendrocytes (Kettenmann et al., 1983) in primary culture.

Based on their findings, Kuffler (1967) and others proposed that glial cells mediate several important physiological processes related to interstitial K^+ levels. Castellucci and Goldring (1970) and Cohen (1970, 1974) demonstrated that glial cells can generate extracellular field potentials in response to changes in extracellular K^+ concentration, $[K^+]_o$. In addition, Orkand et al. (1966) proposed that glial cells may play an important role in regulating $[K^+]_o$ levels through the mechanism of K^+ spatial buffering. Both of these processes are dependent on glial cell membrane being selectively permeable to K^+.

Since this work, experimental and theoretical studies of field potential generation and of K^+ spatial buffering have been conducted on the assumption that K^+ conductance is distributed uniformly across the surface of glial cells. Yet, the ability of glia to generate field potentials or to regulate $[K^+]_o$ might be significantly altered if K^+ conductance were distributed nonuniformly over the cell (Newman and Odette, 1984).

Recent experiments have suggested that in one specialized type of astrocytic glial cell, the Müller cell of the vertebrate retina, K^+ conductance may, in fact, be distributed nonuniformly over the cell surface. Current source-density analysis of the electroretinogram (ERG) b-wave (Newman, 1979, 1980) indicated that light-evoked current efflux from Müller cells was restricted to the cell's endfoot, a process lying adjacent to the vitreous humor in the proximal retina. This finding led us to propose that a disproportionate fraction of the total membrane conductance of Müller cells is localized in the endfoot process (Newman, 1979). A similar suggestion was offered by Tomita and his colleagues based on their studies of field potentials generated by spreading depression episodes (Mori et al., 1976a, b) and by intra-retinal injection of K^+ (Fujimoto and Tomita, 1981; Yanagida and Tomita, 1982).

The present study addresses this hypothesis directly. Using intracellular recordings from amphibian Müller cells, I have determined the distribution of K^+ conductance across the surface of these glial cells. Microdissection and focal K^+ ejection techniques have been employed in measuring the membrane conductance of localized regions of the Müller cell surface. Müller cell membrane selectivity to different ion species has also been determined. Preliminary reports of some of these findings have appeared previously (Newman, 1981, 1984).

Materials and Methods

Animals. Müller cell recordings were made from the leopard frog, *Rana pipiens*, and from the tiger salamander, *Ambystoma tigrinum mavortium*.

Retinal slice. Retinal slices of both frog and salamander retinas were prepared as described by Werblin (1978). Dark-adapted eyes were hemisected and the back half was cut into smaller squares. These retinal pieces were placed vitreal side down on squares of filter paper (Scheicher & Schuell membrane filter), and the sclera, choroid, and pigment epithelium were peeled off, leaving an isolated retina. The filter paper and retina were submerged in a perfusion chamber filled with Ringer's solution and were sliced into 150-μm sections using a tissue chopper. Slices were attached to the bottom of the perfusion chamber (a glass microscope slide) with beads of petroleum jelly so that their cut faces were oriented upward. A coverglass fixed 3.5 mm above the glass slide formed the top of the perfusion chamber.

Received November 8, 1984; Revised January 30, 1985;
Accepted February 5, 1985

[1] I wish to thank Janice I. Gepner and Stephen A. Raymond for their valuable comments on the manuscript. This research was supported by National Institutes of Health Grant EY 04077.

The meniscus between the coverglass and the slide formed two of the "sides" of the chamber.

The chamber was perfused by a gravity feed system supplied from one of several reservoirs. Perfusate was removed from the chamber by suction. The chamber contained 0.5 ml of perfusate and was perfused at a rate of 12 ml/min when switching between Ringer's solutions of differing composition.

Retinal slices were viewed directly at × 200 magnification through the Nomarski optics of a compound microscope and through a video system attached to the microscope trinocular. Normal microscope illumination was used, which thoroughly light-adapted the retinal sections. Retinal layers were clearly visible and identifiable (see Fig. 1). Micropipettes were advanced toward the slices from the two open sides of the perfusion chamber and were oriented parallel to the retinal layers. Recordings were made from retinal slices within 4 hr of excision.

Dissociated cells. Dissociated Müller cells from salamander retinas were prepared by the method of Bader et al. (1979). Isolated retinas were incubated for 30 min in bicarbonate-buffered Ringer's solution containing papain (0.35 mg/ml; Cooper Biomedical, no. 3126) and L-cysteine (0.4 mg/ml). The retinas were then washed in fresh Ringer's solution and separated by gentle trituration with a Pasteur pipette. Solutions were changed several times during the trituration procedure. The last fraction obtained, after the small remaining pieces of retinal tissue were dispersed, generally contained many Müller cells. If trituration was too harsh, Müller cells were broken into small pieces.

When first observed, approximately 5 min after isolation, dissociated Müller cells possessed some, but not all, of the fine cellular processes that extend from the main body of these cells *in vivo*. These remaining processes were resorbed into the trunk of the cells within the following minutes. It is not known whether other cell processes were broken off during the isolation procedure or whether they were retained during dissociation and quickly resorbed.

The dissociated cells were pipetted into a perfusion chamber similar to that used for retinal slices. It differed only in that the glass slide forming the bottom of the chamber was coated with concanavalin A in order to anchor the dissociated cells: a solution of concanavalin A (0.7 mg/ml; Sigma C-2010) in 1 M NaCl was applied to and allowed to dry on the gelatin-coated surface of glass slides. The slides were rinsed in distilled water prior to use. Recordings were made from isolated cells within the first 2 to 3 hr following dissociation.

Solutions. Retinal slices and dissociated cells were perfused in oxygenated bicarbonate-buffered Ringer's and HEPES-buffered Ringer's solutions. The bicarbonate Ringer's contained (in millimolar concentration): NaCl, 82.5; $NaHCO_3$, 27.5; KCl, 2.5; $MgCl_2$, 1.0; $CaCl_2$, 1.8; dextrose, 10.0, equilibrated with 5% CO_2 in O_2 (pH 7.5). The HEPES-Ringer's contained: NaCl, 109.6; KCl, 2.5; $MgCl_2$, 1.0; $CaCl_2$, 1.8; dextrose, 7.4; HEPES, 2.9, equilibrated with 100% O_2, adjusted with KOH to pH 7.5. Results using the two solutions were similar except that intracellular recordings, particularly from dissociated cells, appeared to be more stable in bicarbonate Ringer's. Except when otherwise noted, experiments were performed using the bicarbonate Ringer's.

In some experiments the K^+ concentration of the perfusate was altered by substituting KCl for equimolar amounts of NaCl. Na^+-free Ringer's was made by substituting choline chloride for NaCl. Low Cl^- Ringer's was prepared by substituting $NaSO_4$ for NaCl.

Localized $[K^+]_o$ increases were generated by pressure-ejecting a high $[K^+]$ Ringer's solution from an extracellular pipette. These pipettes had tip diameters of approximately 1 μm and were filled with a 100 mM KCl solution. Pressure (1 to 5 psi) was applied through a General Valve Corp. Picospritzer II.

Recording. All experiments were conducted at room temperature (18 to 22°C). Intracellular recordings from retinal slices were made with omega-dot micropipettes filled with 4 M K^+ acetate or K^+ citrate. Electrode impedance generally ranged from 80 to 120 megohms. Recordings from dissociated Müller cells were made with patch clamp electrodes used in the whole cell recording configuration (Hamill et al., 1981). The tips of the heat-polished patch electrodes were approximately 3 μm in diameter. Patch electrodes were filled with 100 mM KCl. Intracellular recordings from both preparations were amplified through a W-P Instruments KS-700 preamplifier.

Intracellular recordings were referenced to an Ag/AgCl wire immersed in the perfusion chamber. When Müller cells were bathed in low Cl^- Ringer's, voltages were recorded differentially between the intracellular pipette and a similar extracellular pipette filled with 3 M KCl.

Cell responses were recorded on a chart recorder and a digital oscilloscope and stored on disc in a microcomputer which could digitally subtract and average multiple traces.

Special care was taken when measuring the input impedance of Müller cells from the retinal slice preparation. This proved difficult because cell resistance (4 to 8 megohms) was significantly lower than electrode resistance. Constant current pulses (generally ranging from 0.1 to 1.0 nA) were passed through the micropipette and a bridge circuit (internal to the preamplifier). Identical current pulses were passed through the pipette immediately following electrode withdrawal, and any residual bridge inbalance (due to a change in electrode resistance) was digitally subtracted from the previous intracellular record. Impedance records were discarded if electrode resistance changed significantly during a cell penetration.

The subtraction procedure was not necessary when measuring the input resistance of dissociated cells. The low resistance of the patch electrodes used in these experiments (approximately 5 megohms) made impedance measurements of these cells straightforward.

The time constant of responses to injected current pulses was determined by the method of Trachtenberg and Pollen (1970). Cell responses were displayed on an oscilloscope along with the pulse response of an RC network consisting of a variable resistor in parallel with a capacitor. The time constant of the network was adjusted until it matched that of the cell response.

Measurement of surface area. Dissociated salamander Müller cells were prepared and perfused as described above. Drawings of individual cells were traced by hand from the screen of a video monitor at × 1440 magnification. In order to estimate surface area, cells were assumed to be cylindrically symmetric. The width of a cell (diameter of the cell cylinder) was measured at 3.5-μm intervals along the entire length of the cell. The areas of all of the cylindrical segments plus the areas of the top (the distal end) and the bottom (the proximal face of the endfoot) of the cell were added to obtain the total surface area. The distal end of the cell is composed of microvillar projections which were estimated to double the actual surface area in this region of the cell (based on responses to K^+ ejections, see "Discussion"). Thus, the measured surface area of the distal end of the cell was doubled for purposes of calculating total cell surface area.

Results

Frog retinal slices. Intracellular Müller cell recordings were made from frog retinal slices perfused with HEPES-Ringer's (Fig. 1). Cells were penetrated with intracellular electrodes aligned with the middle of the inner nuclear layer (where Müller-cell cell bodies are located), thus maximizing the probability of obtaining stable Müller cell penetrations.

Müller cell penetrations were identified by their large resting membrane potentials, which averaged −90.6 ± 3.9 mV (n = 17) in stable recordings. (Mean values ± SD are given in this paper.) Müller cell penetrations were also confirmed in preliminary experiments by the iontophoretic injection of the fluorescent dye Lucifer Yellow into cells having large resting potentials. These injections revealed a cell morphology typical of Müller cells. Müller cell recordings from retinal slices could frequently be held for more than 1 hr.

K^+ selectivity of Müller cells. The selectivity of Müller cell membrane to K^+ was determined by monitoring changes in the cell membrane potential, E_m, as the K^+ concentration of the perfusate was altered. In response to a step increase in the $[K^+]$ of the perfusate, cells depolarized, reaching a new stable level within 2 to 3 min (Fig. 2). When $[K^+]_o$ was raised above 10 mM, Müller cells sometimes depolarized rapidly and then gradually repolarized to a new stable level. This transient depolarization, indicated by the *arrow* in Figure 2, is presumably due to neuronal release of K^+ during an episode of spreading depression. The maximum depolarization reached during these transient responses was −42 ± 5 mV (n = 8).

Results from one perfusion experiment on a single cell are illustrated in Figure 3. As shown by the *solid circles* in Figure 3, Müller cell E_m varied linearly with log ($[K^+]_o$) over an extremely wide range of perfusate $[K^+]$. The data were fit by a straight line having the Nernstian slope of 59 mV/decade change in $[K^+]_o$.

E_m deviated from the ideal K^+ voltage only for very low values of $[K^+]_o$, below approximately 2.5 mM. As in other types of cells, this deviation could be due to an Na^+ conductance. This was tested by fitting the data points with the voltage predicted by the Goldman equation (incorporating both K^+ and Na^+ permeabilities; Goldman, 1943). An $[Na^+]_o$ of 112 mM and an $[Na^+]_i$ of 10 mM were assumed

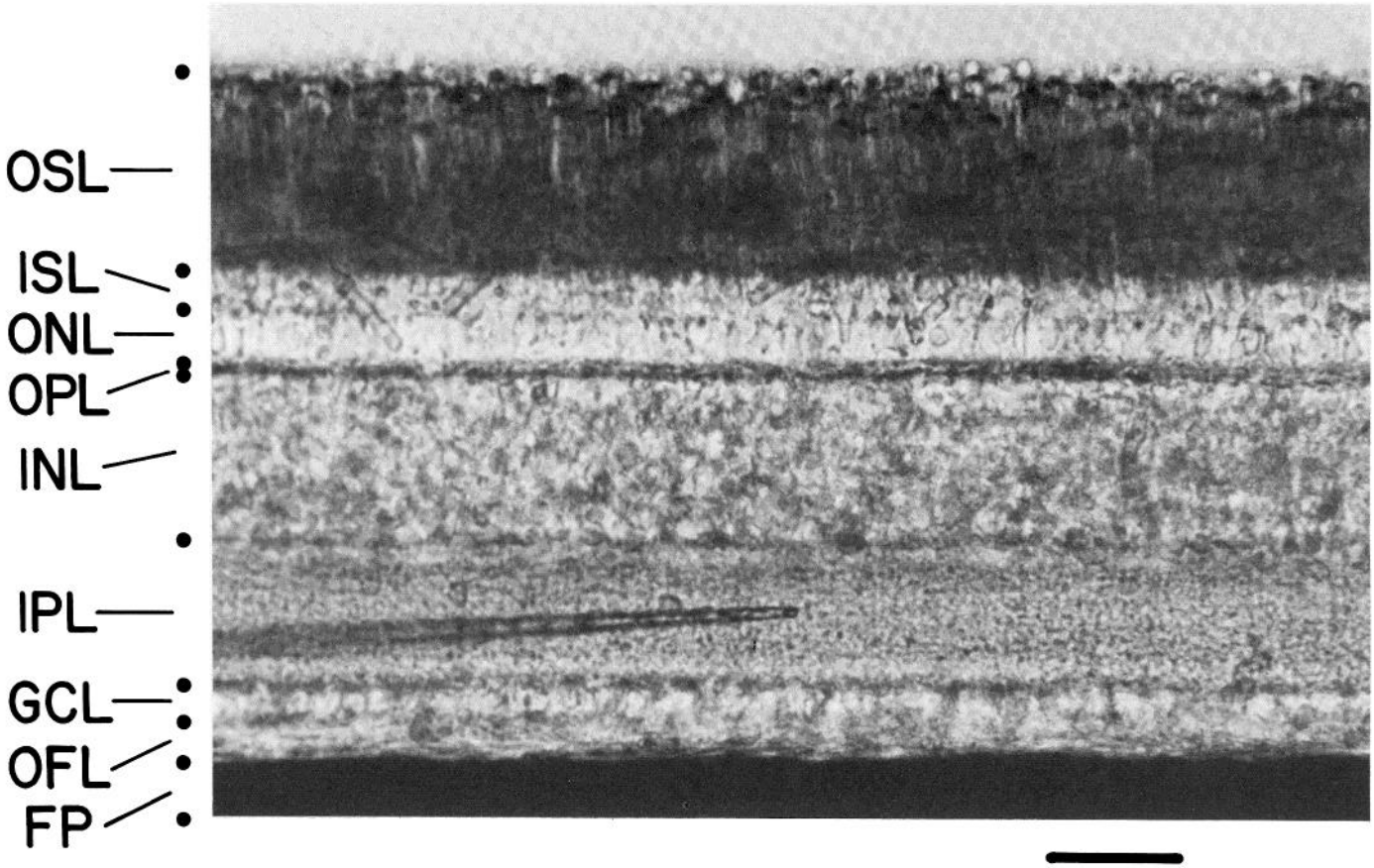

Figure 1. Brightfield photomicrograph of frog retinal slice. The tip of a K^+ ejection pipette is pressed against the cut surface of the inner plexiform layer. Retinal layers are indicated at *left*: *OSL*, outer segment layer; *ISL*, inner segment layer; *ONL*, outer nuclear layer; *OPL*, outer plexiform layer; *INL*, inner nuclear layer; *IPL*, inner plexiform layer; *GCL*, ganglion cell layer; *OFL*, optic fiber layer; *FP*, filter paper, upon which the retinal slice is lying. *Scale bar*, 50 μm.

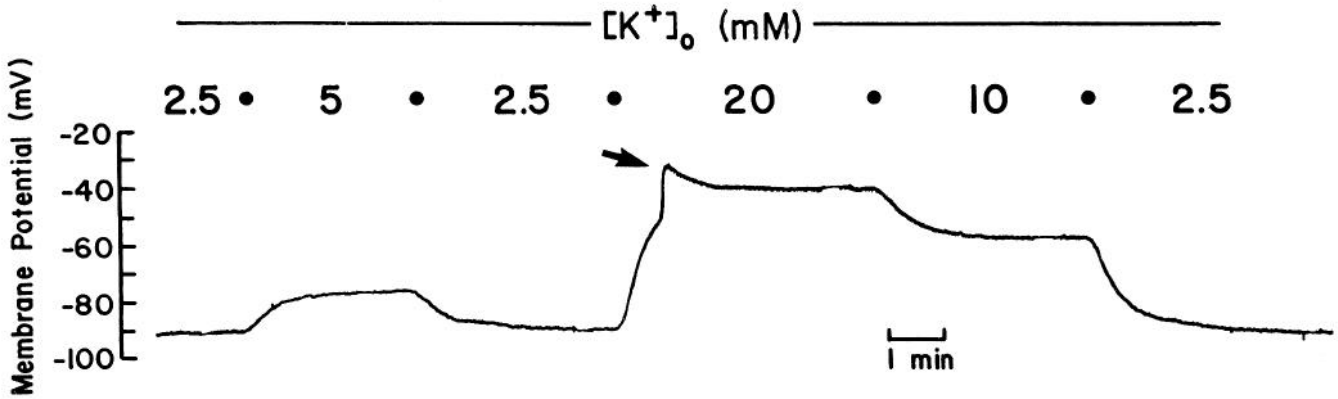

Figure 2. Recording of Müller cell membrane potential as perfusate $[K^+]_o$ is varied (frog retinal slice preparation). Perfusate $[K^+]$ is indicated *above* the *trace*. Transient depolarization triggered by addition of 20 mM K^+ (*arrow*) reflects a spreading depression episode.

for these calculations. As seen in Figure 3 (*curved line*) an excellent fit was obtained for this cell when a K^+:Na^+ permeability ratio of 435:1 was used.

If the deviation of E_m from the K^+ equilibrium potential is due to Na^+ conductance, this deviation should be eliminated if Na^+ flux is also eliminated. This was accomplished by substituting choline for Na^+ in the perfusate. As shown in the *open circles* of Figure 3, the deviation of E_m from the K^+ equilibrium potential was virtually eliminated when the same cell was bathed in Na-free perfusate.

K^+ perfusion experiments in normal perfusate were conducted on a total of 12 cells with similar results obtained in all cases. Each perfusion series was fit by the Goldman equation. The average value of the K^+:Na^+ permeability ratio obtained was 490 ± 100:1. Perfusion experiments in Na-free Ringer's were performed on seven cells with results similar to that shown by the *open circles* in Figure 3 obtained in all cases.

Retinal slices were also perfused in low Cl^- Ringer's in order to determine whether the Müller cell membrane was permeable to Cl^-. When $[Cl^-]_o$ of the perfusate was reduced from 90.6 to 8.1 mM, Müller cell E_m changed less than 0.3 mV (n = 9). In addition, no significant change in Müller cell input resistance was measured when Müller cells were bathed in low Cl^- Ringer's (n = 4).

Ouabain. The effect of the Na^+/K^+ ATPase inhibitor ouabain on the membrane potential of Müller cells was determined in the frog retinal slice. HEPES-Ringer's containing 10^{-5} M ouabain (Sigma 0-3125) was used. In the four cells tested, introduction of ouabain caused

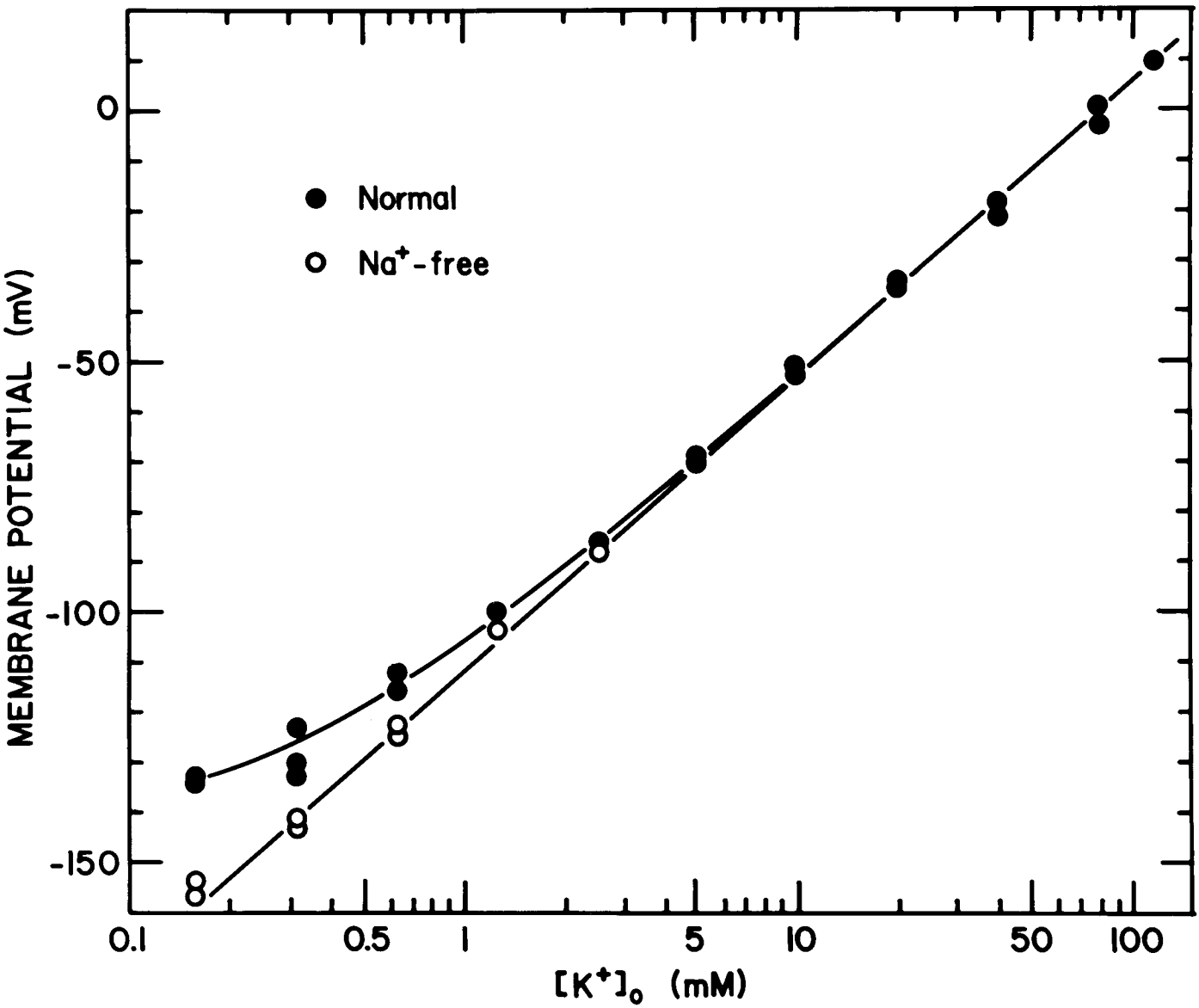

Figure 3. Frog Müller cell membrane potential as a function of perfusate $[K^+]$. All data are from a single cell in the retinal slice preparation. ●, normal Ringer's; O, Na^+-free Ringer's. The data are fit by a *straight line* having a slope of 59 mV/decade and a *curved line* representing the E_m values predicted by the Goldman equation (K^+:Na^+ permeability ratio = 435:1).

an initial rapid depolarization followed by a slower continuous depolarization. The initial depolarization ranged from 2.5 to 5 mV in amplitude and occurred within 1 to 2 min of the introduction of the drug. Following this initial phase, the cell continued to depolarize at a rate of 0.4 to 2.1 mV/min. This slow depolarization was monitored for more than 30 min in some cells and could be partially reversed by washing out the ouabain with fresh Ringer's. Following ouabain removal, cell depolarization was either halted or reversed, but cells never repolarized completely to their initial membrane potential.

Müller cell impedance in retinal slices. Müller cell input resistance was measured in frog retinal slices bathed in HEPES-Ringer's. Müller cells were penetrated in two retinal laminae, in the inner nuclear layer, where Müller-cell cell bodies are located, and in the optic fiber layer, where Müller cell endfoot processes lie. When cells were penetrated in their cell bodies, a mean resistance of 8.5 ± 0.7 megohms was measured (n = 44). When cells were penetrated in their endfeet, a resistance of 4.8 ± 1.0 megohms was found (n = 14).

Responses to K^+ ejections in retinal slices. The regional distribution of Müller cell K^+ conductance was studied by monitoring cell depolarizations generated by localized increases in $[K^+]_o$. The rationale for this experimental approach is that the amplitude of cell depolarization produced by such a $[K^+]_o$ increase is directly proportional to the conductance of that portion of the membrane experiencing the $[K^+]_o$ increase. This relation is derived formally in the "Appendix."

Intracellular recordings were made from Müller cells in both salamander and frog retinal slices. Cells were penetrated in their cell bodies, in the inner nuclear layer of the slice. In salamander slices, only cells that lay within the first 30 μm below the cut surface of the slice were used. In frog slices, cells lying within the top 100 μm of the slice were used.

Localized $[K^+]_o$ increases were produced at the cut surface of the slice by pressure-ejecting a 100 mM KCl solution from extracellular pipettes. A pipette was lowered until it compressed the cut surface of the slice. K^+ solution was forced into the slice as pressure was applied to the pipette.

When a Müller cell was penetrated, its position within the slice could not be determined visually because the pipette tip was not visible. The location of the penetrated cell was determined, instead,

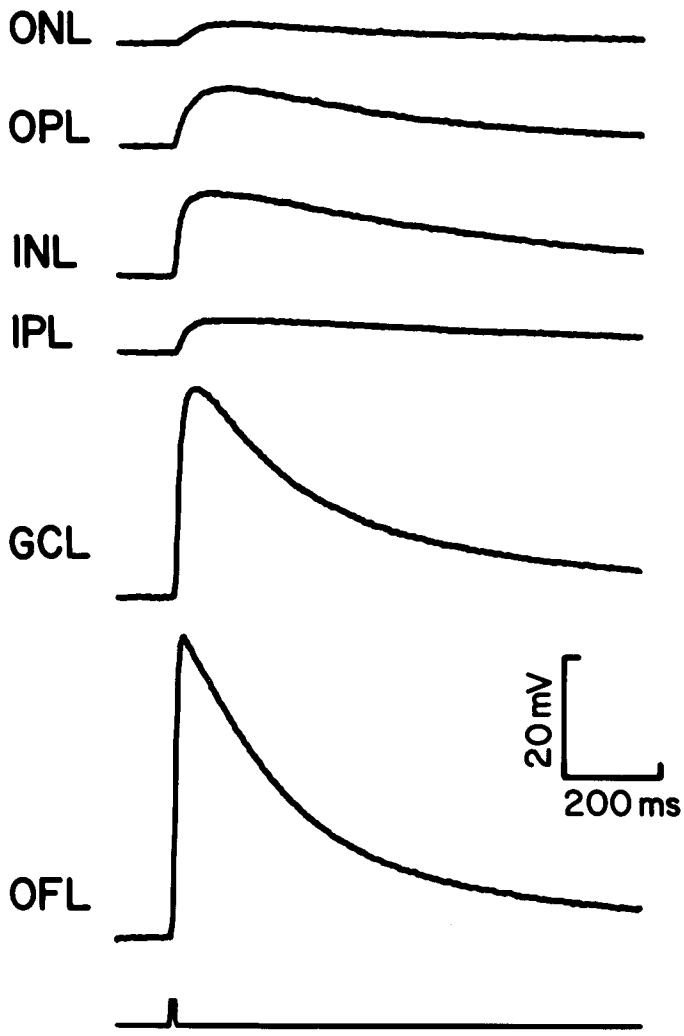

Figure 4. Müller cell responses to localized $[K^+]_o$ increases recorded from the salamander retinal slice preparation. The cell was penetrated in the inner nuclear layer. Labels indicate the site of K^+ ejection (*abbreviations* are defined in the legend to Fig. 1). The onset and duration of the pressure pulse applied to the ejection pipette are indicated at the *bottom*.

by identifying the position on the surface of the slice where K^+ ejection produced a cell depolarization having a minimum latency. The K^+ ejection pipette was then positioned successively over different retinal laminae, with the pipette tip always remaining in line with the Müller cell being monitored. K^+ was ejected from the pipette at each location and the resulting Müller cell depolarization was recorded. For a given cell, equal amounts of K^+ were ejected from the pipette at each retinal location.

The results of one such K^+ ejection series in a salamander slice are illustrated in Figure 4. K^+ ejection in the optic fiber layer produced a cell depolarization of 49 mV, whereas ejections in the ganglion cell, inner plexiform, inner nuclear, outer plexiform, and outer nuclear layers produced depolarizations of 35, 5.5, 14, 9.5, and 3.5 mV, respectively.

A summary of the amplitudes of responses evoked by localized K^+ ejections in both salamander and frog retinal slices is given in Table I. In both preparations, K^+ ejections in the optic fiber layer evoked responses that were approximately twice as large as those generated by ejections in the ganglion cell layer (roughly 14 μm away) and 2 to 17 times larger than were responses to ejections in other retinal laminae.

Responses to K^+ ejections at a single retinal location were generally quite reproducible, even when the ejection pipette was moved between trials. This was not true for K^+ ejection responses in the optic fiber layer. The amplitude of optic fiber layer responses sometimes varied as much as 50% when the ejection pipette was moved only a few micrometers. One had the impression that the K^+-sensitive region of the cell within the optic fiber layer was restricted to a very small area.

Dissociated salamander Müller cells. The K^+ ejection responses described above may not reflect the true distribution of K^+ conductance along the Müller cell surface because different regions of the cell membrane might not be equally accessible to the ejected K^+. A tortuous diffusion pathway between the slice surface and the Müller cell membrane in a particular retinal layer might cause a reduction in the depolarization evoked by a K^+ ejection in that layer. Indeed, the variations in the time courses of the K^+ responses seen in Figure 4 suggest that there are differences in membrane accessibility within the retinal slice.

This problem was circumvented by repeating the K^+ ejection experiments on dissociated Müller cells, which had membrane surfaces that were directly accessible to ejected K^+. Experiments were performed on dissociated cells of the salamander which proved easier to isolate and record from than cells of the frog.

A photograph of a dissociated salamander cell is illustrated in Figure 5. Visible are the following Müller cell structures: (*a*) the distal end of the cell, which lies at the outer limiting membrane in the intact retina; (*b*) the cell body, lying in the inner nuclear layer; (*c*) the stalk region, which extends through the inner plexiform layer; (*d*) the lateral surface of the endfoot, which lies within the optic fiber layer; and (*e*) the proximal surface of the endfoot, which lies against the inner limiting membrane in the intact retina.

Responses to K^+ ejections in dissociated Müller cells. Müller cell responses were recorded with patch electrodes attached to the cell body region of isolated cells. An extracellular pipette filled with 100 mM KCl was positioned against specific regions of the Müller cell surface (see Fig. 5). K^+ ejected from the pipette raised $[K^+]_o$ locally and produced a localized membrane depolarization which was recorded in the cell body.

The results of one series of K^+ ejections is shown in Figure 6. A

TABLE I

Summary of Müller cell K^+ response amplitudes

K^+ response amplitudes ± SD are given as a percentage of the optic fiber layer response amplitude and the proximal endfoot response amplitude. The sample size is indicated in parentheses.

Preparation	Optic Fiber Layer	Ganglion Cell Layer	Inner Plexiform Layer	Inner Nuclear Layer	Outer Plexiform Layer	Outer Nuclear Layer
Retinal slice						
Ambystoma	100	46 ± 22 (9)	25 ± 13 (15)	22 ± 10 (13)	24 ± 15 (11)	8 ± 4 (7)
Rana	100	53 ± 16 (8)	53 ± 15 (8)	13 ± 6 (8)	9 ± 5 (4)	6 ± 2 (8)
	Proximal Endfoot	Lateral Endfoot	Stalk	Cell Body		Distal End
Dissociated Cell						
Ambystoma	100	15.0 ± 10.4 (17)	2.8 ± 1.1 (17)	2.0 ± 0.9 (17)		4.2 ± 3.4 (17)

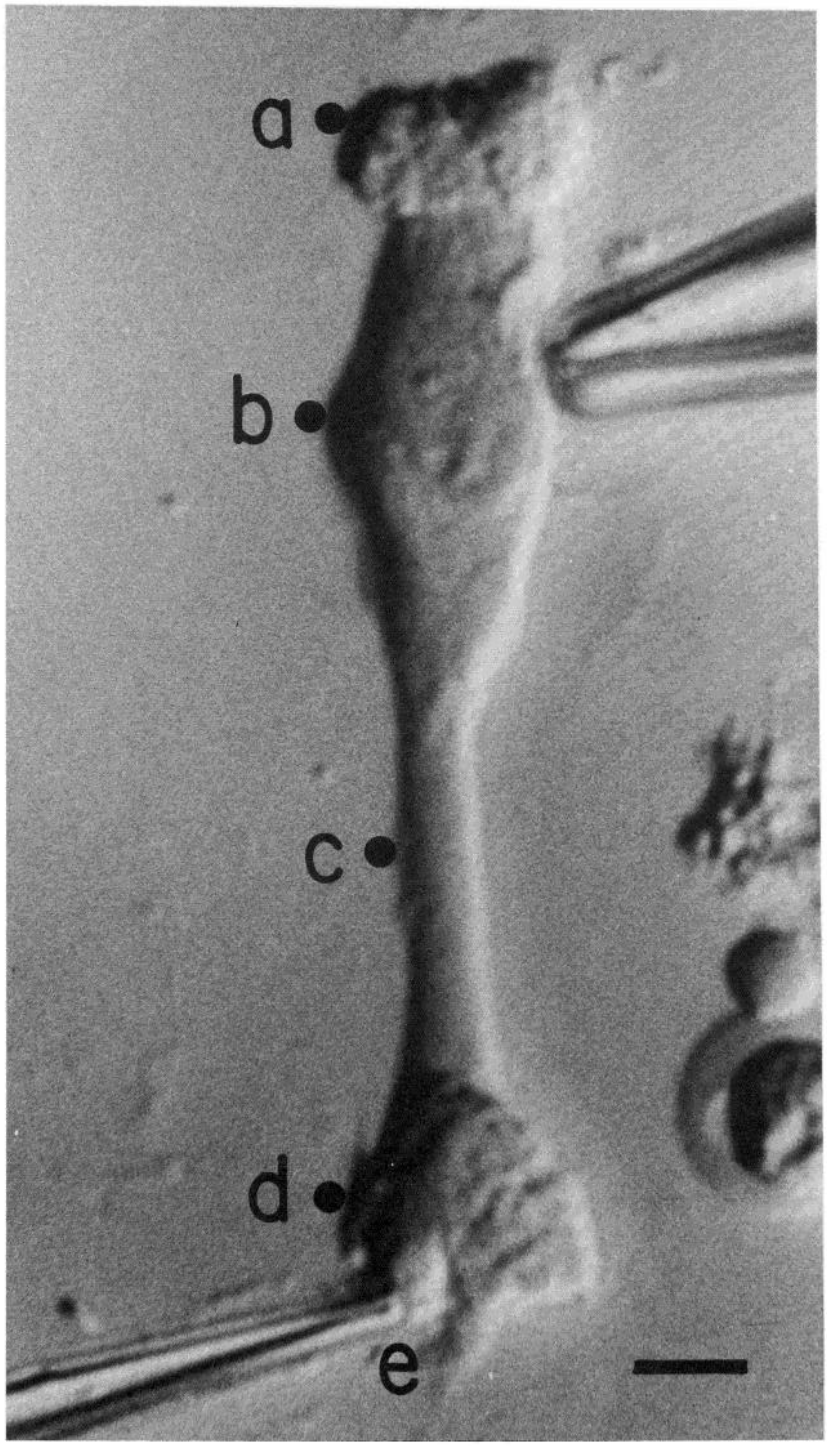

Figure 5. Photomicrograph of a dissociated salamander Müller cell with a patch electrode attached to the cell body (*upper right*). A K^+ ejection pipette lies against the proximal face of the endfoot (e). *Solid circles* indicate typical locations of the K^+ ejection pipette used in K^+ ejection experiments. *a*, Distal end; *b*, cell body; *c*, stalk; *d*, lateral face of endfoot; *e*, proximal face of endfoot. *Scale bar*, 10 μm.

5-msec pulse of K^+ ejected at the proximal surface of the endfoot (Fig. 6*e*) generated a transient 26.8-mV response. When the ejection pipette was moved to the lateral face of the endfoot, a distance of only 15 μm, the response to the same 5-msec pulse of K^+ was reduced 12.8-fold to 2.1 mV (Fig. 6*d*). K^+ ejections directed at more distal regions of the cell (Fig. 6, *a* to *c*) produced responses 0.4 to 1.1 mV in amplitude. This variation in response amplitude cannot be due to response attenuation along the length of the Müller cell: the largest response was generated at a location most distant from the recording electrode.

These responses are replotted in Figure 7 so that their peaks are normalized to the same amplitude. All five responses peak at approximately the same time. *Traces a*, *b*, and *e* in Figure 7 all have similar time courses. The secondary depolarizations seen in *traces c* and *d* are due to diffusion of ejected K^+ to the endfoot surface. The similarity of the initial time courses of these responses indicates that ejected K^+ had equal access to the Müller cell surface for all five ejection locations.

Similar results were obtained in a total of 17 dissociated salamander cells. Ejections directed at the proximal surface of the endfoot produced responses 6.7 times larger than did ejections directed at the lateral endfoot surface (a mean distance of only 11.5 μm away) and 24 to 50 times greater than did ejections directed at other regions of the cell. K^+ ejection responses were quite repeatable, even when the ejection pipette was repositioned between trials. This

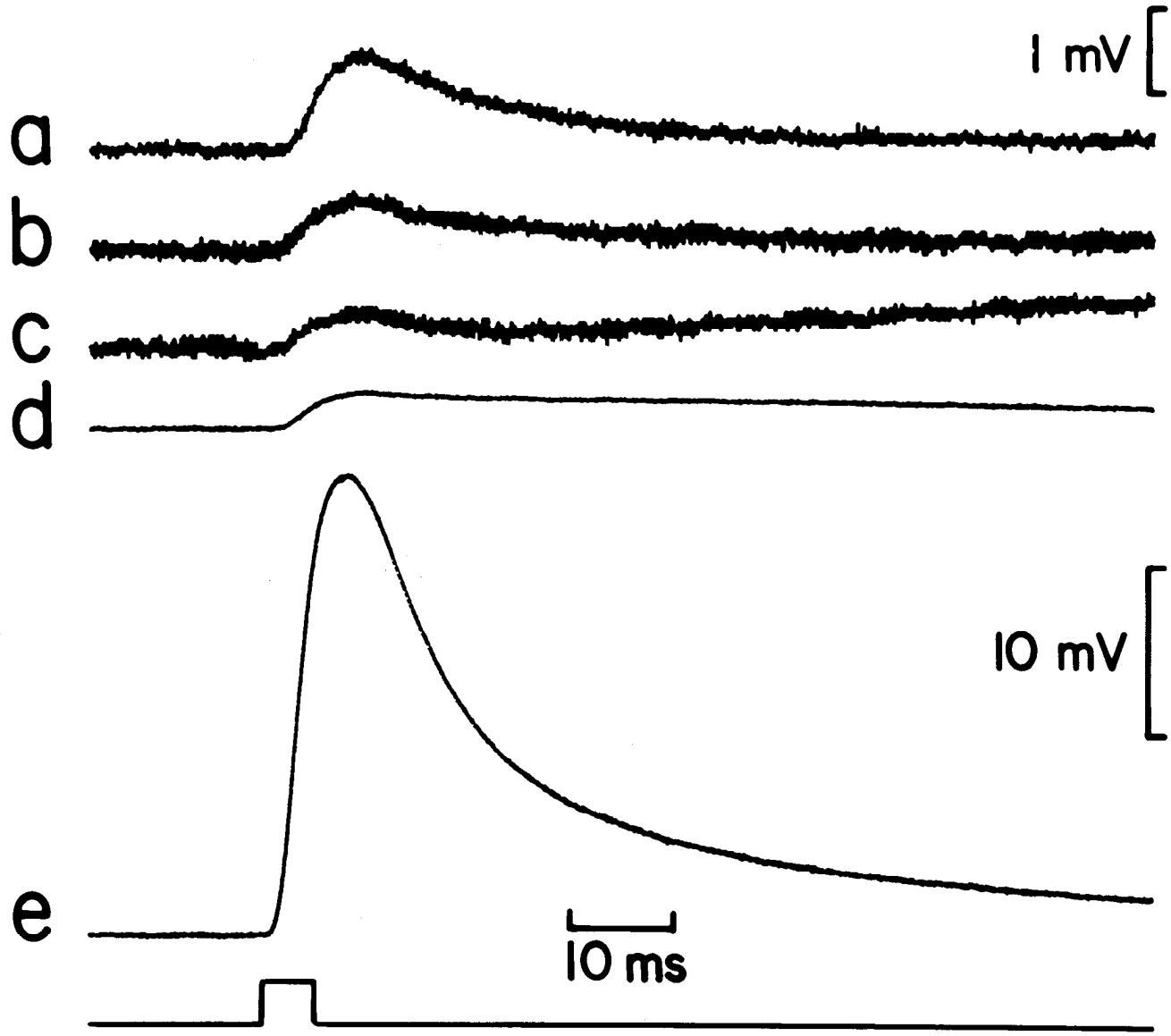

Figure 6. Müller cell responses to localized $[K^+]_o$ increases recorded from the cell body of a dissociated salamander cell. Labels correspond to the sites of K^+ ejection, as indicated in Figure 5. The onset and duration of the pressure pulse are indicated at the *bottom*. *Traces a* to *c* are expanded vertically 5-fold relative to *traces d* and *e*. Each *trace* is an average of four sweeps.

was true for all five locations on the Müller cell surface. K^+ response results from dissociated cells are summarized in Table I.

K^+ ejection responses were also recorded from dissociated Müller cells bathed in perfusate containing 10^{-5} M ouabain. As described above, ouabain treatment leads to cell depolarization. However, the ratio of response amplitudes evoked by ejections directed at different cell regions remained largely unchanged. K^+ ejections directed at the proximal face of the endfoot generated cell depolarizations 6 to 41 times greater than did ejections directed at other cell regions in these ouabain-treated cells ($n = 3$).

Impedance of dissociated Müller cells. If a significant fraction of total Müller cell membrane conductance lies in the endfoot process of the cell, removing this structure should cause an increase in cell input resistance. This was tested by measuring the input resistance of dissociated salamander Müller cells before, during, and after surgical dissection of the cell.

The input resistance of individual cells was measured with patch electrodes attached to the cell body. While monitoring cell impedance in the cell body, the stalks of these cells were cut by compression with a glass needle (see Fig. 8). The cell membrane potential dropped to near zero as the stalk was severed and then, in many cases, began to repolarize as the cut end of the stalk resealed. A large increase in the input resistance of the remaining portion of the cell was measured within seconds of the visually observed resealing of the stalk and the onset of repolarization.

An intracellular record made during the dissection of one such cell is shown in Figure 9. Following stalk section (Fig. 9, *arrow*), E_m fell from −86 mV to −13 mV and then, over the next 10 min, repolarized to −78 mV. In other cases, cells repolarized to E_m values ranging from −42 to −101 mV.

The impedance records made from one dissected cell are shown in Figure 10, *A* and *B*. In the intact cell (Fig. 10*A*) an input resistance of 7.3 megohms and an input time constant of 0.83 msec were measured. Following removal of the endfoot process (Fig. 10*B*), the cell resistance rose 22-fold to 160 megohms while the cell time constant increased 21-fold to 17.7 msec. Because of the large increase in cell resistance following stalk section, the amplitude of the current pulses used to measure cell impedance was reduced from 1 nA to 0.1 nA.

A total of 14 *A. tigrinum* Müller cells were dissected in this manner. Cell resistance rose an average of 21-fold to 164 ± 82 megohms when the endfoot process was removed while the cell time constant rose 19-fold to 13.5 ± 6.8 msec in these cells.

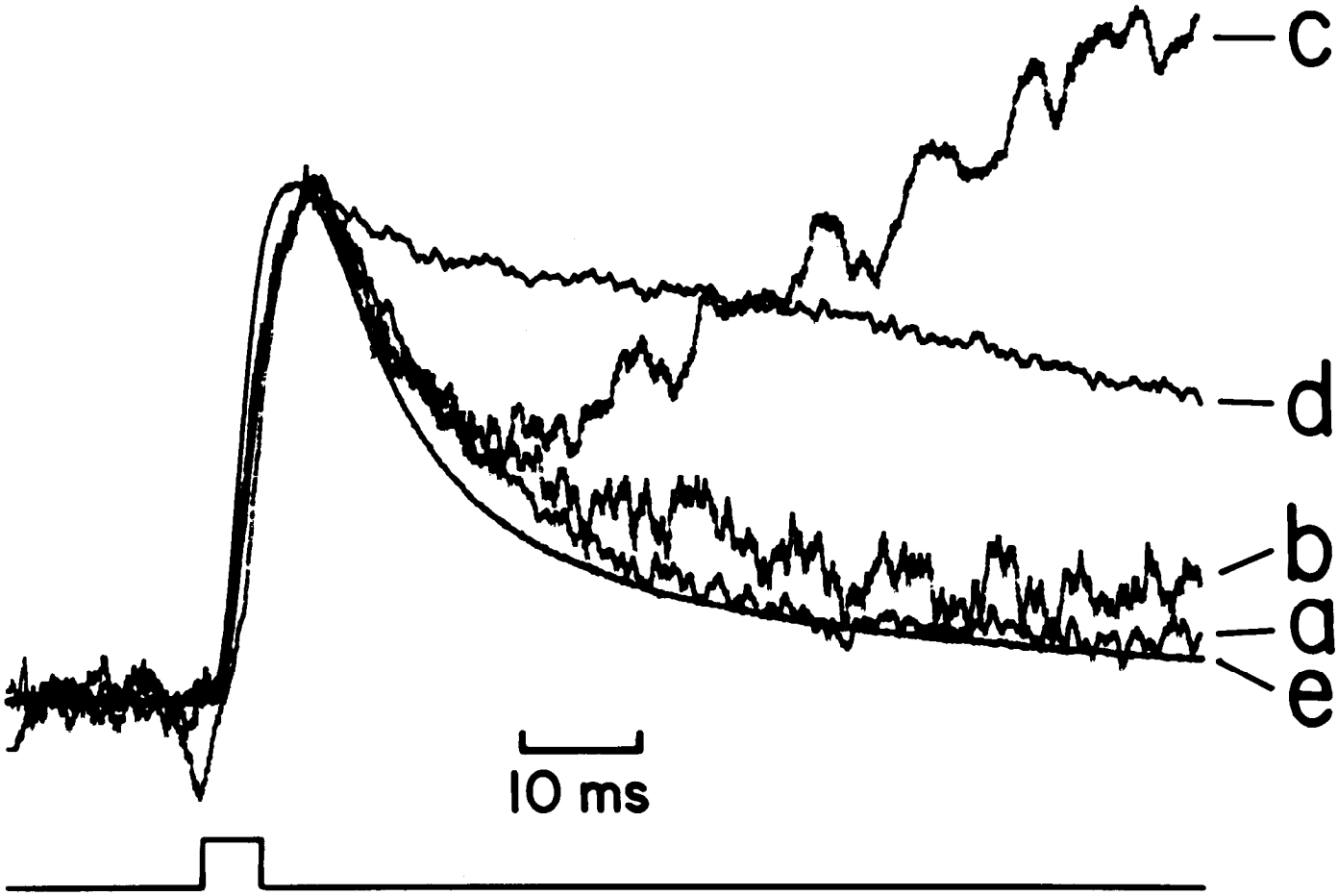

Figure 7. Müller cell K^+ responses of Figure 6 normalized to the same peak amplitude. *Traces a* to *d* have been smoothed by a moving window averaging routine. The time to peak of *traces a* to *d* is approximately 8.7 msec; the time to peak of *trace e* is 8.1 msec.

A second series of impedance measurements of endfoot-shorn cells was obtained in a somewhat different manner. The dissociation procedure used to prepare isolated Müller cells produced a significant number of cells that were missing their endfeet. The endfeet of these cells were presumably sheared off during trituration of the retina. These endfoot-less cells often retained their stalk processes and thus were more "intact" and perhaps healthier than were the surgically prepared endfoot-shorn cells, the stalks of which were often resorbed into the cell body following section.

The input impedance of this "self-prepared" population of endfoot-shorn cells was measured with patch electrodes attached to the cell body. The input resistance and time constant values measured in these *A. tigrinum* cells were similar to the values measured from endfoot-shorn cells prepared by microdissection. The mean input resistance of these cells was 135 ± 64 megohms while the cell time constant was 10.9 ± 6.3 msec ($n = 10$). The results both from this sheared population of endfoot-less Müller cells and from the microdissected population were combined and are given in Table II.

Impedance of isolated endfeet. It is possible that the high input resistance measured in endfoot-shorn Müller cells does not accurately reflect the normal, *in situ* properties of the cell but is caused by the mechanical disruption of the cell membrane or, perhaps, by a change in the ionic composition of the cytoplasm. This possibility was tested by measuring the input impedance of isolated endfoot processes prepared by the same microdissection procedure used to isolate cell bodies.

The response of one such isolated endfoot to an applied current pulse, recorded at a fast sweep speed, is shown in Figure 10*D*. This record was obtained by patching onto the endfoot process of an intact cell and then cutting the stalk of the cell. The record was made immediately after the proximal end of the cut stalk resealed and the endfoot process repolarized (to −93 mV). The input resistance of this isolated endfoot was 12.3 megohms and the time constant was 0.11 msec. The impedance record of an intact cell, recorded at the same sweep speed, is shown in Figure 10C for comparison.

Results from a series of endfoot recordings are given in Table II. When the distal half of the cell was surgically removed, leaving only the endfoot and proximal half of the stalk, the mean cell resistance rose to 14.9 megohms, whereas the mean cell time constant fell to 0.17 msec. The relatively small difference in cell resistance between intact cells and isolated endfeet demonstrates that surgical disruption of the stalk membrane does not, in itself, lead to a large increase in cell input resistance.

Recordings made from the isolated endfeet of dissociated cells were not as stable as those made from intact cells or from isolated cell bodies. Endfoot recordings were often accompanied by swelling or other changes in appearance of the endfoot process. These visual changes were accompanied by a steady increase in cell input resistance, suggesting that the conductance of the endfoot membrane was being disrupted by the electrode recording. The input resistance of isolated endfeet often increased from approximately 10 megohms to several hundred megohms within a matter of minutes. Such increases in cell resistance were not observed when patch electrodes were attached to the cell bodies of intact cells or endfoot-less cells.

This lability of endfoot conductance probably accounts for most of the difference between the cell input resistance measured in intact cells (7.9 megohms) and the resistance measured in isolated endfeet (14.9 megohms). Even in the most stable endfoot penetra-

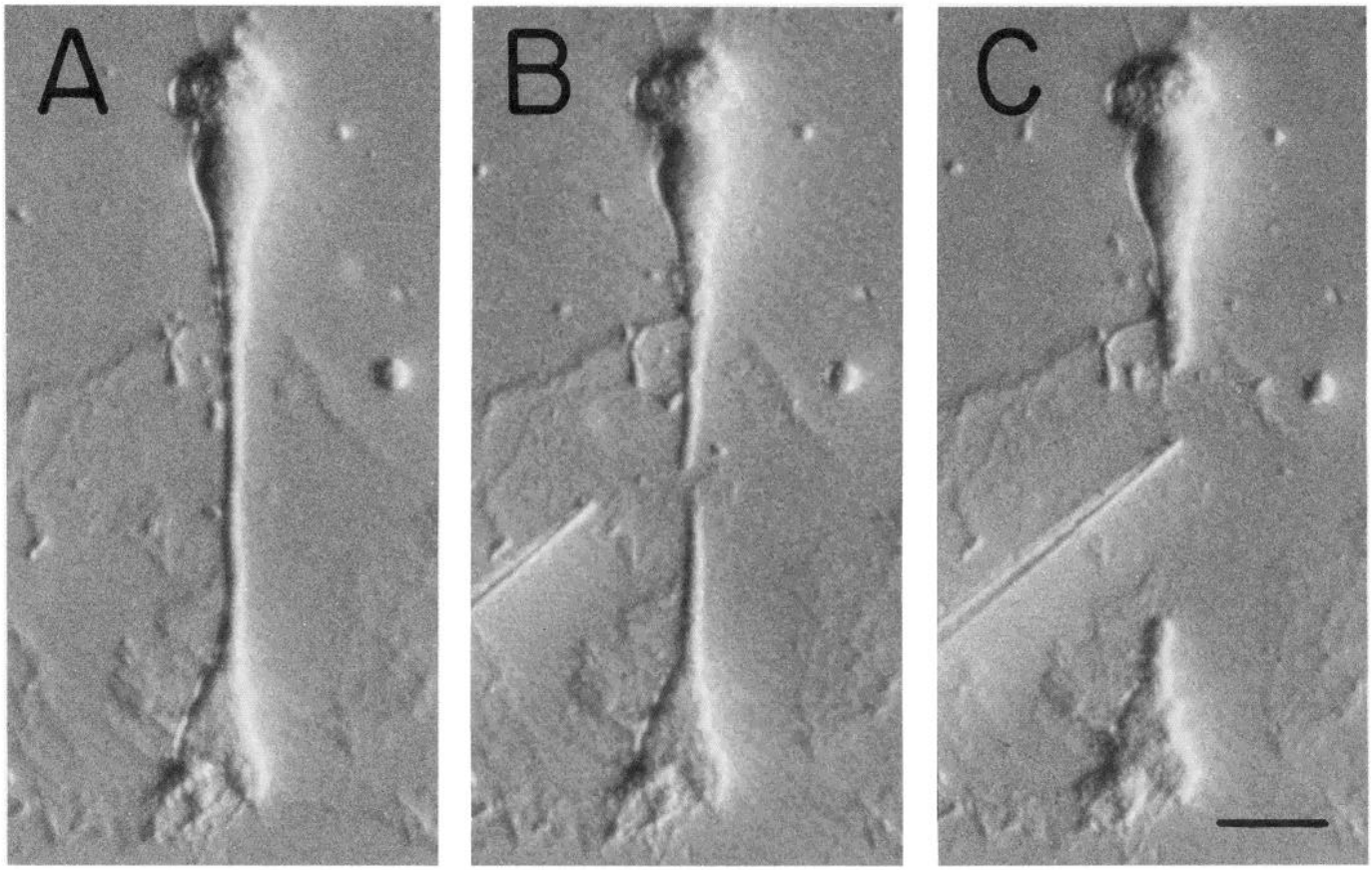

Figure 8. Photomicrographs of a dissociated salamander Müller cell microdissected with a glass needle. *A*, Intact cell. *B*, Fifteen seconds after the stalk was cut with the needle (shown at *left*). The cut ends of the stalk have resealed. *C*, Several minutes later. The cut ends of the stalk have retracted back toward the cell body and the endfoot (at *bottom* of photograph). *Scale bar*, 20 μm.

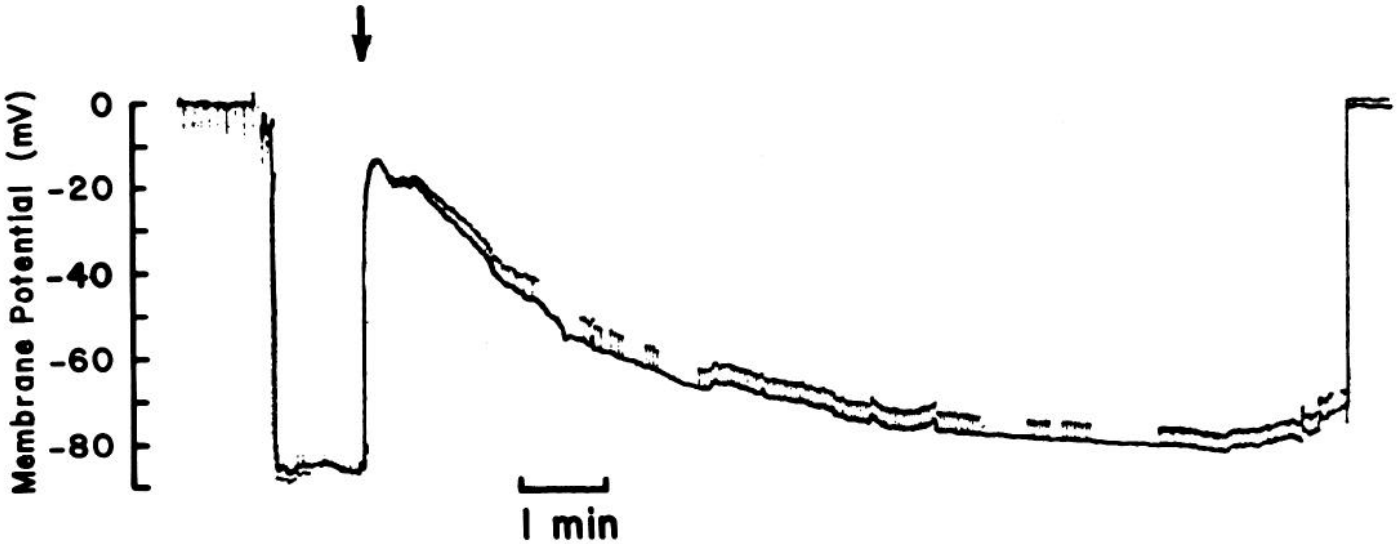

Figure 9. Recording of Müller cell membrane potential during the microdissection procedure. The initial hyperpolarization occurs when the dissociated salamander cell is penetrated in the cell body region. (This particular cell was recorded with a conventional intracellular electrode rather than with a patch clamp electrode.) Following a brief period, the stalk is cut and the cell depolarizes (*arrow*). The cut end of the stalk quickly reseals and the cell body repolarizes over a 10-min period. The final depolarization to 0 mV occurs when the recording electrode is withdrawn from the cell. The *interrupted line* above the *trace* was formed by transient depolarizations generated by the injection of constant current pulses. The amplitudes of these depolarizations increase as the cut stalk reseals, indicating an increase in cell input resistance.

tions, the mechanical disruption of the isolated endfoot process caused by the patch electrode probably destroyed some of the conductance of the endfoot.

Surface area of Müller cells. The surface area of dissociated salamander Müller cells was measured by a graphic method described under "Materials and Methods." The total surface area averaged 5540 ± 590 μm^2/cell (n = 14). The surface area of the proximal face of the endfoot averaged 442 ± 137 μm^2 (n = 14).

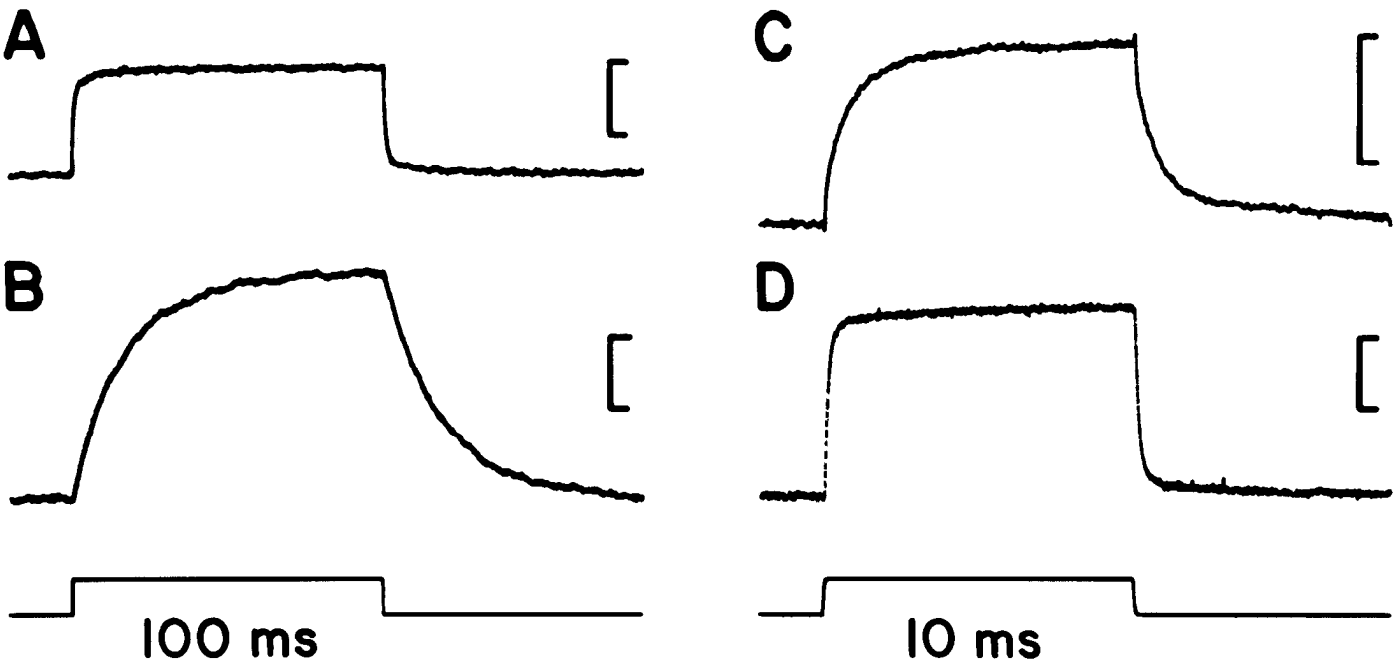

Figure 10. Depolarizations evoked by current pulses applied to dissociated salamander Müller cells. *A*, Response of an intact cell. Current pulse, 1 nA. *B*, Response from the same cell after the stalk was cut, removing the endfoot process. Current pulse, 0.1 nA. The input resistance of the cell increased from 7.3 to 160 megohms and the time constant increased from 0.83 to 17.7 msec following removal of the endfoot process. *C*, Response of an intact cell, recorded from the cell body region, shown at a faster sweep speed. Current pulse, 1 nA. *D*, Response from an isolated endfoot process of a cell the stalk of which was previously cut. Current pulse, 1 nA. Note the fast time constant of the response recorded from the endfoot (0.11 msec). *Scale bar* in all cases, 5 mV. The time courses of the current pulses are indicated at the *bottom*. *Trace D* is an average of four sweeps.

TABLE II

Summary of impedance measurements from dissociated Ambystoma Müller cells

Values ± SD are given for cell input resistance, cell time constant, and cell capacitance. The state of the cell is indicated in column 1. The sample size (n) is given in parentheses. Capacitance values are calculated from the relation: capacitance = time constant/resistance.

State of Cell	Resistance (megohms)	Time Constant (msec)	Capacitance (pF)
Intact cell (n = 27) (Electrode on cell body)	7.9 ± 2.4	0.70 ± 0.37	98 ± 62
Isolated cell body (n = 24)	152 ± 75	12.4 ± 6.6	85 ± 32
Cell Body/Intact ratio	19.2	17.7	0.87
Isolated endfoot (n = 9)	14.9 ± 4.7	0.17 ± 0.06	11.7 ± 3.3
Endfoot/Intact ratio	1.7	0.24	0.12

Rasmussen (1975), in an electron microscopic study of cells in the intact retina, found Müller cell surface area to vary from 2,038 μm^2 in the grass snake to 20,325 μm^2 in gecko. The value of 5,540 μm^2 measured in the present study probably underestimates the true surface area of dissociated salamander Müller cells because it was assumed that, except for the distal end of the cell, the cell surface was entirely smooth. The surface area of salamander Müller cells *in vivo* must be larger still because they contain many cell processes which are resorbed when the cells are isolated.

Discussion

K^+ selectivity of Müller cells

One of the characteristic features of glial cells is their membrane selectively for K^+ (Orkand, 1977). Results from the ion substitution experiments described here demonstrate that Müller cells, as well, have membranes which are highly selective for K^+. An estimate based on fitting the data with the Goldman equation suggests that the ratio of K^+ to Na^+ permeabilities in Müller cells is 490:1. Similar measurements made in cultured oligodendrocytes indicate that the K^+ conductance is 200 times greater than the Na^+ conductance in these cells (Kettenmann et al., 1983).

Glial cells of the leech have been shown to have appreciable Cl^- conductance as well as K^+ conductance (Walz and Schlue, 1982). A reduction of $[Cl^-]_o$ in these invertebrate cells is followed by cell depolarization and an increase in cell input resistance. In contrast, as described here, *R. pipiens* Müller cells experience negligible changes in E_m and input resistance when $[Cl^-]_o$ is reduced, indicating that its membrane is largely impermeable to Cl^-. Glial cells of other vertebrate species have also been shown to be impermeable to Cl^- (Kettenmann et al., 1983; Walz et al., 1984).

Recent experiments in cultured astrocytes (Walz et al., 1984) and oligodendrocytes (Kettenmann et al., 1983) demonstrate that these cells do not behave as ideal K^+ electrodes when $[K^+]_o$ is raised, even though their membranes are exclusively permeable to K^+. This occurs because increases in $[K^+]_o$ trigger a net uptake of K^+ which increases intracellular $[K^+]$. As demonstrated in the present study, Müller cells do behave as ideal K^+ electrodes for $[K^+]_o$ greater than 2.5 mM. This suggests that, unlike some other types of glia, Müller cells do not take up K^+ when $[K^+]_o$ is raised, at least during the exposure times used in the present study (2 to 3 min).

Distribution of K^+ conductance

The most important finding of this study concerns the strikingly nonuniform distribution of K^+ conductance across the Müller cell

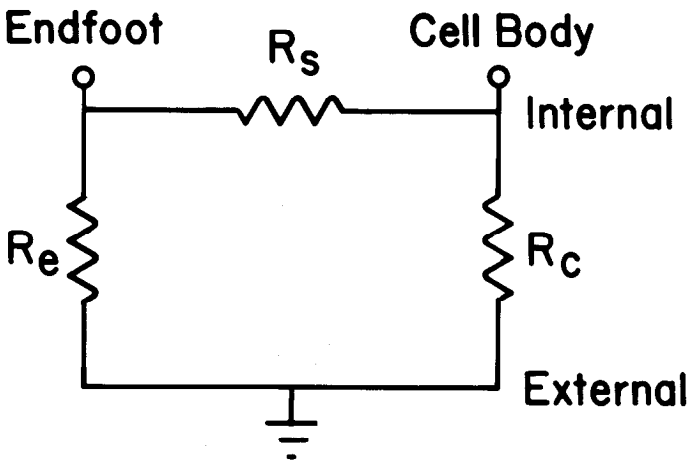

Figure 11. Ohmic model of a Müller cell used to analyze the input resistance measurements from frog and salamander cells. R_e, endfoot membrane resistance; R_c, cell body membrane resistance; R_s, internal longitudinal resistance of the stalk. The two nodes at the *top* of the circuit represent the locations where cell resistance is measured with electrodes in the endfoot or cell body regions of the cell.

surface. This membrane specialization has been demonstrated for both *Ambystoma* and *Rana* cells using microdissection and focal K^+ ejection techniques in both retinal slice and dissociated cell preparations.

Impedance measurements

The most direct measure of regional differences in membrane conductance comes from resistance measurements of dissociated cells. Intact dissociated *A. tigrinum* cells have an input resistance of 7.9 megohms, whereas endfoot-shorn cells have a resistance of 152 megohms. The two methods used to remove the endfoot process, microdissection and shearing during dissociation, yield similar results.

The fraction of total cell conductance remaining in the cell body following endfoot removal can be calculated by taking the conductance (1/resistance) ratio of endfoot-shorn to intact cells: (1/152)/(1/7.9) = 0.05, for *A. tigrinum* cells. Thus, 95% (1 − 0.05) of total *Ambystoma* Müller cell membrane conductance lies in the shorn-off portion of the cell, in or near the endfoot.

The high conductance of the Müller cell endfoot process was confirmed in resistance measurements made in the frog retinal slice preparation. Cell body penetrations yielded a Müller cell input resistance of 8.5 megohms, whereas endfoot penetrations yielded a value of 4.8 megohms. This difference demonstrates that the conductance of the endfoot region is greater than the conductance of the cell body. The magnitude of this conductance difference depends on the resistive coupling between the two cell regions.

Figure 11 illustrates a circuit which was used in analyzing these results. Here, a frog Müller cell is modeled by two membrane regions representing the endfoot (R_e) and cell body (R_c) portions of the cell. They are coupled by an internal resistance (R_s) representing the resistance of the stalk region. From the experimental measurements, we know that the equivalent resistance of the circuit, as measured at the endfoot node, is 4.8 megohms whereas the resistance measured at the cell body node is 8.5 megohms.

Let us assume that the cell body membrane (R_c) has a total resistance of 100 megohms (probably an underestimate). Solution of the circuit equations then yields an endfoot resistance, R_e, of 5.0 megohms and a stalk resistance, R_s, of 4.3 megohms. These calculated values are relatively insensitive to changes in our initial assumption. For instance, assuming R_c values ranging from 50 to 200 megohms, R_e will vary from 5.3 to 4.9 megohms.

Based on an endfoot resistance of 5.0 megohms and a cell body resistance of 100 megohms, one can calculate that in the *Rana* retinal slice preparation 95% of total Müller cell conductance lies in the endfoot process. If *Rana* cell body resistance is greater than the 100 megohms that was initially assumed, the percentage of total cell conductance in the endfoot would be even greater than 95%.

Responses to K^+ ejections

Dissociated cells. Responses of dissociated cells to K^+ ejections can be used to obtain quantitative estimates of local K^+ conductance in Müller cells. As demonstrated in the "Appendix," the amplitude of the response produced by a focal K^+ ejection is directly proportional to the conductance of the membrane region being depolarized. This relation can be used to calculate the ratio of the specific membrane conductances of different regions of the Müller cell surface.

The mean values of K^+ response amplitudes recorded from dissociated salamander Müller cells are given in Table I. Using these values and equation 2 of the "Appendix," relative specific membrane conductance can be estimated. The results indicate that the specific membrane conductance of the proximal face of the endfoot is 7.6 times greater than the conductance of the lateral face of the endfoot, 41 times greater than the conductance of the stalk, 57 times greater than the conductance of the cell body, and 27 times greater than the conductance of the distal end of the cell.

The cell body membrane makes up a large fraction of the total surface area of the cell. Thus, these results indicate that the specific membrane conductance of the proximal face of the endfoot is approximately 57 times greater than the conductance of most of the remainder of the cell.

The results also show that the specific membrane conductance of the proximal face of the endfoot is manyfold greater than the conductance of the lateral endfoot surface, although these two regions are separated by an average of only 11.5 μm. This demonstrates that the high conductance region of the endfoot is largely restricted in its spatial extent to that part of the cell surface which is directly apposed to the vitreous fluid *in situ*.

Dissociated cells. Estimates of the regional distribution of K^+ conductance based on measurements of isolated Müller cells may not be accurate because of changes in cell membrane properties introduced by the dissociation procedure. Dissociated cells possess few of the fine cellular processes present *in vivo*. Some of these processes are resorbed into the main body of the cell immediately following dissociation. Other processes may be lost during the dissociation procedure. A measurable fraction of the cell conductance could reside in these lost processes. It is also possible that resorption lowers the conductance of the processes. In either case, the measurements made on dissociated cells would underestimate the true, *in vivo* conductance of the cell body region of Müller cells (but see below).

K^+ response of distal end of cell. The distal end of the Müller cell is composed of microvillar extensions (Pedler, 1963) which increase the effective surface area of this cell region. A K^+ ejection directed toward the microvilli would produce a larger K^+ response than a similar ejection directed at the cell body because of the increased surface area. Thus, the actual specific membrane conductance of the distal end of the cell may be smaller than the value indicated by the K^+ ejection responses.

Time course of K^+ responses. Although the time courses of the rising phase and peak of the K^+ responses recorded from different cell regions were similar, they were not identical. As seen in Figure 7, the K^+ response of the proximal endfoot membrane (*e*) peaked slightly earlier than did the responses of other cell regions (7.6 ± 1.4 versus 8.6 ± 2.3 msec; n = 17). This difference in response time course most likely arises because the region of the proximal endfoot surface responding to ejected K^+ is slightly smaller (and thus closer to the ejection pipette) than the cell surface region responding to ejected K^+ in other parts of the cell.

This suggests that the region of high membrane conductance occupies a relatively small area on the endfoot surface and means that the amplitudes of endfoot K^+ responses underestimate the true conductance of the endfoot membrane. (If a larger area of high conductance membrane responded to ejections on the proximal endfoot surface, larger K^+ responses would be generated.)

Retinal slices. The simple relation between K^+ response amplitude and specific membrane conductance derived in the "Appendix" assumes that equal areas of membrane are exposed to $[K^+]_o$ increases having similar magnitudes and time courses. As illustrated by the near identity of the initial time courses of the K^+ ejection responses recorded from isolated cells (Fig. 7), these assumptions are valid for the dissociated cell preparation. These assumptions are not valid, however, for K^+ ejections in retinal slices.

First, there are differences in the diffusion pathway from the site of ejection to the Müller cell surface in retinal slices. K^+ diffusion into the plexiform and nuclear layers is slower than is diffusion onto the endfoot membrane. This accounts for the differences in K^+ response time course seen in Figure 4. A tortuous diffusion pathway reduces the amplitudes of cell body responses relative to endfoot responses. On the other hand, the volume fraction of extracellular space is much smaller within the retinal slice (3 to 13%; Karwoski, et al., 1985) than it is at the endfoot surface (100%). This results in a smaller dilution of ejected K^+ within the slice than at the endfoot membrane and to larger K^+ ejection responses in the cell body region.

In addition, the amplitude of responses evoked by K^+ ejections in the optic fiber layer of retinal slices was extremely sensitive to the location of the ejection pipette, suggesting that there was a restricted area of endfoot membrane with high K^+ sensitivity. In contrast, the K^+ responses in other retinal layers were not very sensitive to the ejection pipette location, implying that a larger membrane surface area was responding to increases in $[K^+]_o$ in these layers.

In short, it is difficult to analyze the results of K^+ ejections in the retinal slice preparation in a quantitative fashion. However, it can be reasonably concluded from the responses recorded in these experiments that the membrane conductance of the endfoot is significantly larger than the conductance of other cell regions.

Specific membrane capacitance

The specific membrane capacitance of dissociated salamander Müller cells can be estimated from the data obtained in this study. Intact cells have a total capacitance of 98 pF/cell and an area of 5540 μm^2. Thus, the cell membrane has a specific capacitance of 1.77 $\mu F/cm^2$. Kettenmann et al. (1984) have measured a nearly identical specific membrane capacitance of 1.7 $\mu F/cm^2$ for cultured mouse oligodendrocytes.

Specific membrane resistance

The specific membrane resistance of the cell body and endfoot regions of salamander Müller cells can be estimated from the impedance measurements made on dissociated cells. Isolated cell bodies (endfoot-shorn cells) have a resistance of 152 megohms and a capacitance of 85 pF (see Table II). Assuming a specific membrane capacitance of 1.77 $\mu F/cm^2$, a specific membrane resistance of 7300 ohm·cm^2 results. This large specific resistance is reflected in the long time constant of isolated cell bodies (12.4 msec; Fig. 10*A*).

Similarly, the resistance and area of the proximal face of the endfoot must be determined in order to calculate the specific resistance of this region of the cell. The absolute resistance of salamander Müller cell endfeet can be estimated using the circuit shown in Figure 11. For dissociated salamander cells, R_c = 152 megohms, R_s = 1 megohm, and the input resistance as measured in the cell body equals 7.9 megohms. This results in an endfoot resistance, R_e, of 7.3 megohms.

The area of the proximal face of the endfoot, where most of the high conductance of the cell is presumably located, equals 442 μm^2. Given a total resistance of 7.3 megohms, this region of the cell has a specific resistance of 32 ohm·cm^2. This value can be compared to the specific resistance of the frog node of Ranvier, which is a region of membrane having a high density of K^+ channels. The frog nodal membrane at rest, which is largely permeable to K^+ (g_{leak}), has a specific resistance of approximately 25 ohm·cm^2 (Hille, 1984).

The low specific resistance of the endfoot membrane accounts for the short time constant of isolated endfeet measured in this study (0.17 msec; Fig. 10*D*). This time constant would actually be severalfold shorter still if isolated endfoot processes could be prepared so that they contained only the low resistance endfoot membrane and none of the high resistance membrane of the stalk or lateral face of the endfoot.

Based on an endfoot specific resistance of 32 ohm·cm^2 and a cell body specific resistance of 7300 ohm·cm^2, the ratio of the specific resistances of the two regions of the Müller cell is estimated to be 1:228. This ratio is somewhat higher than the 1:57 value of specific resistances which was obtained from the K^+ response results analyzed above. The reason for the discrepancy between these two values is not clear, although the difference may be partially due to difficulties in measuring membrane conductance accurately in the K^+ ejection experiments. If, as suggested above, K^+ ejection responses underestimate the conductance of the endfoot membrane, the calculated ratio of specific resistances would actually be greater than 1:57. In any event, both the impedance measurements and the K^+ response experiments leave little doubt that the specific membrane resistance of the endfoot process is a great deal smaller than the specific resistance of the remainder of the cell.

Estimates of the specific membrane resistance of other types of astrocytes fall between the values of the specific resistance of the endfoot and cell body regions of Müller cells: astrocytes in cat neocortex, 193 to 482 ohm·cm^2 (Trachtenberg and Pollen, 1970) and 603 ohm·cm^2 (Glotzner, 1973); cultured astrocytes, 326 ohm·cm^2 (Trachtenberg et al., 1972) and 2000 to 3000 ohm·cm^2 (Kimelberg, 1983). It is possible that the specific membrane resistances measured in these cells do not represent the true specific resistance of any single patch of membrane but rather represent an average of a high resistance cell body membrane and a low resistance endfoot membrane. (The "averaged" specific membrane resistance of dissociated Müller cells calculated from the impedance measurements made on intact cells in this study is 438 ohm·cm^2.

Nature of endfoot conductance

The physical substrate underlying the high K^+ conductance of the endfoot membrane is not known, although a high density of passive K^+ channels is a likely possibility. Raviola (1977) has demonstrated in a freeze-fracture study of the monkey retina that there is a high concentration of orthogonal arrays of intramembranous particles (assemblies) on the Müller cell endfoot membrane which is directly apposed to the vitreous. Assemblies are also found on those surfaces of endfeet of brain astrocytes which face the capillaries and the pial surface (Landis and Reese, 1974). The function of these assemblies is not known. However, their distribution closely matches the distribution of high K^+ conductance in Müller cells, suggesting that assemblies may contain K^+ channels. (It should be noted that assemblies in amphibian Müller cells and astrocytes are not found in high concentrations as they are in mammals; Landis and Reese, 1981; Wujek and Reier, 1984).

It was noted above that the K^+ conductance of the endfoot process was susceptible to damage produced by the patch clamp electrodes and by swelling. Input resistance rose when the endfoot was mechanically stressed. Assemblies are similarly susceptible. The normal distribution of assemblies within the endfoot membrane of astrocytes is disrupted by mechanical stress occurring during cell dissociation (Anders et al., 1983). This is additional evidence linking the presence of assemblies with high K^+ conductance.

Function of high endfoot conductance

The primary finding of this study is that the membrane conductance of Müller cells is distributed in a remarkably nonuniform manner across the cell surface: 95% of the cell conductance is localized in the endfoot process. The results further indicate that this high conductance region is largely restricted to the proximal surface of the endfoot, that portion of the cell which is directly apposed to the vitreous fluid *in situ.* This conductance distribution has important

consequences for the regulation of K^+ levels in the retina and for the generation of the electroretinogram.

K^+ spatial buffering. An important function of glial cells in the central nervous system is to regulate $[K^+]_o$ by the process of K^+ spatial buffering (Orkand et al., 1966; Gardner-Medwin, 1983). As suggested by Orkand et al. (1966), K^+ enters glial cells in regions of tissue where $[K^+]_o$ is raised. In order to maintain electrical neutrality, an equal amount of K^+ exits from these cells, or from cells electrically coupled to them, in regions where $[K^+]_o$ is lower. A return current flow through extracellular space completes the circuit. The net effect of this current flow is to transfer K^+ from regions of tissue where $[K^+]_o$ is high to regions where $[K^+]_o$ is lower.

The high conductance of the Müller cell endfoot makes spatial buffering a far more powerful process than previously envisioned. In the absence of a membrane specialization, spatial buffering by Müller cells would redistribute localized increases in light-evoked $[K^+]_o$ evenly throughout the retina. Because of the endfoot specialization, however, almost all of the K^+ current entering Müller cells in regions of $[K^+]_o$ increase would be shunted out through the endfoot process into extracellular space at the vitreal surface of the retina. The vitreous would function as an enormous K^+ sink, storing excess K^+ until retinal $[K^+]_o$ levels returned to normal. K^+ could then be transferred back to the retina from the vitreous by a reversal of the K^+ current flow.

This directed flow of spatial buffer current, termed K^+ siphoning (Newman et al., 1984), has been demonstrated experimentally. Newman et al. (1984) exposed the distal end of dissociated salamander Müller cells to increased $[K^+]_o$ and monitored K^+ efflux from other regions of the cell with K^+-selective microelectrodes. K^+ efflux was only detected at the proximal face of the endfoot, indicating that most of the K^+ current entering the cell at the site of $[K^+]_o$ increase exited from the endfoot region. Based on the finding of the present study that 95% of the total cell membrane conductance is localized to the endfoot, it follows that *in situ* 95% of all excess K^+ transferred by Müller cells is siphoned into the vitreous.

Astrocytes. A similar K^+ siphoning process may operate in the brain. Astrocytes, like Müller cells, possess endfoot processes. They surround the capillaries and lie adjacent to the pial surface of the brain. If astrocyte endfeet, like those of Müller cells, have high K^+ conductance, they would serve an important role in brain K^+ homeostasis. K^+ current entering astrocytes in regions of increased $[K^+]_o$ would be shunted out through the endfoot processes, directly into the blood plasma or the cerebrospinal fluid instead of into neighboring neural tissue. The endothelial cells of brain capillaries are largely impermeable to K^+ (Cohen et al., 1968). However, K^+ deposited at the outer surfaces of these cells by astrocytic K^+ siphoning might be actively transported by the endothelial cells into the capillary septum.

Generation of field potentials. The high conductance of the Müller cell endfoot also influences the generation of field potentials in the retina. The b-wave, d-wave, M-wave, and slow PIII components of the ERG are believed to be generated by radially directed K^+ currents flowing through Müller cells (Faber, 1969; Miller and Dowling, 1970; Karwoski and Proenza, 1977; Kline et al., 1978; Newman, 1980; Newman and Odette, 1984). Müller cell endfoot conductance plays a dominant role in determining the course that these currents follow through extracellular space. The length and density of these current pathways determine, in turn, the amplitudes of the ERG potentials. For example, computer simulations indicate that the Müller cell produces an ERG b-wave potential 5 times larger than would be generated if the endfoot process had the same specific K^+ conductance as the remainder of the cell (Newman and Odette, 1984).

High conductance in the endfeet of astrocytes would influence the generation of field potentials in the brain in a similar fashion. Astrocytes are known to depolarize in response to $[K^+]_o$ increases (Grossman and Hampton, 1968; Ransom and Goldring, 1973; Kelly and Van Essen, 1974) and are believed to generate some brain potentials (Castellucci and Goldring, 1970; Kuffler, 1967; Cohen, 1970, 1974). The location of high conductance astrocyte endfeet would determine the dipole orientation of extracellular potentials generated by these cells. The field potentials generated by currents shunted through the endfeet surrounding capillaries would tend to cancel due to their radial orientation. In contrast, the endfeet forming the glia limitans at the surface of the brain are all oriented in the same direction. K^+ currents shunted through these endfeet would generate negative slow potentials that could be measured by electrodes within active regions of gray matter (and referenced to the surface of the brain; see Cordingley and Somjen, 1978).

Appendix

The relationship between Müller cell responses to focal K^+ ejections and the specific conductance of the cell membrane may be derived by using the ohmic model of a Müller cell illustrated in Figure 12. This idealized cell is composed of n membrane segments, each representing a different region of the cell surface. Each segment has a membrane conductance, g_i. The conductance of the proximal face of the endfoot is represented by g_1. All membrane segments except the endfoot segment (g_2 through g_n) are assumed to be coupled together by an internal space having zero resistivity. This is a good approximation of the cell body-distal end of the cell which should remain isopotential due to its large internal volume.

The endfoot membrane region will not remain isopotential with the remainder of the cell following a localized depolarization because it is coupled to the cell body by the long stalk process. The resistance of the stalk is modeled in the equivalent circuit by resistance $1/g_s$. It has the value 4.3 megohms for *Rana* cells (see calculations under "Discussion") and a value of 1.0 megohm for the stouter stalks of

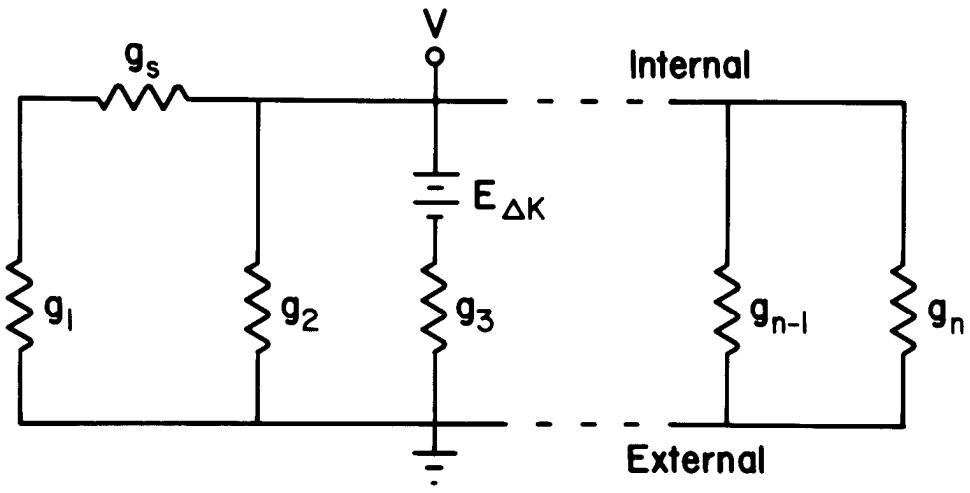

Figure 12. Ohmic model of Müller cell used to analyze results from K^+ ejection experiments. The cell is divided into n membrane segments, each having conductance g_i. The high K^+ conductance region of the endfoot is represented by g_1. The internal longitudinal conductance of the stalk is represented by g_s. $E_{\Delta K}$ represents the membrane depolarization evoked by a localized K^+ ejection.

Ambystoma Müller cells (diameter 4.5 μm, length 30 μm for *Ambystoma* versus diameter 2.5 μm, length 40 μm for *Rana*).

The effects of a localized $[K^+]_o$ increase can be modeled by introducing a voltage source ($E_{\Delta K}$) in series with one of the membrane segments. This battery represents the local change in the K^+ equilibrium potential generated by a focal $[K^+]_o$ increase. If membrane segment i is depolarized, the response of the cell, V_i, will equal $E_{\Delta K} \cdot g_i / \Sigma g_n$. (In calculating Σg_n, the sum of the conductances of all membrane segments in parallel, the value of g_1 is actually g_1 in series with g_s.) If a membrane segment j is depolarized, the cell response V_j will equal $E_{\Delta K} \cdot g_j / \Sigma g_n$. The ratio of the two responses is

$$V_i/V_j = g_i/g_j \quad (1)$$

Thus, we obtain the simple relation that the amplitude of a response produced by a localized K^+ ejection is directly proportional to the conductance of the membrane segment being depolarized.

When calculating the relative conductance of the proximal face of the endfoot (segment 1), the conductance of the stalk must be included in the relation

$$V_1/V_j = (g_1 \text{ in series with } g_s)/g_j \quad (2)$$

For the calculations performed in this study, g_1 was set to 1/(7.3 megohms) and g_s to 1/(1 megohm). Thus, the conductance of the proximal face of the endfoot (relative to the conductance of other cell regions) is 1.14 times greater [(7.3 + 1)/7.3] than is indicated by the amplitude of the proximal endfoot K^+ response.

References

Anders, J. J., P. M. Blessing, and M. W. Brightman (1983) Freeze-fracture analysis of plasma membranes of isolated astrocytes from rat brain. Brain Res. *278:* 81–91.

Bader, C. R., P. R. MacLeish, and E. A. Schwartz (1979) A voltage-clamp study of the light response in solitary rods of the tiger salamander. J. Physiol. (Lond.) *296:* 1–26.

Castellucci, V. F., and S. Goldring (1970) Contribution to steady potential shifts of slow depolarization in cells presumed to be glia. Electroencephalogr. Clin. Neurophysiol. *28:* 109–118.

Cohen, M. W. (1970) The contribution by glial cells to surface recordings from the optic nerve of an amphibian. J. Physiol. (Lond.) *210:* 565–580.

Cohen, M. W. (1974) Glial potentials and their contribution to extracellular recording. In *Handbook of Electroencephalography and Clinical Neurophysiology*, A. Remond, ed., pp. 43–59, Elsevier-North Holland Publishing Co., Amsterdam.

Cohen, M. W., H. M. Gerschenfeld, and S. W. Kuffler (1968) Ionic environment of neurones and glial cells in the brain of an amphibian. J. Physiol. (Lond.) *197:* 363–380.

Cordingley, G. E., and G. G. Somjen (1978) The clearing of excess potassium from extracellular space in spinal cord and cerebral cortex. Brain Res. *151:* 291–306.

Faber, D. S. (1969) Analysis of slow transretinal potentials in response to light. Ph.D. thesis, State University of New York, Buffalo.

Fugimoto, M., and T. Tomita (1981) Field potentials induced by ejection of potassium ion into the frog retina: A test of current interpretations of the electroretinographic (ERG) b-wave. Brain Res. *204:* 51–64.

Gardner-Medwin, A. R. (1983) Analysis of potassium dynamics in mammalian brain tissue. J. Physiol. (Lond.) *335:* 393–426.

Glotzner, F. L. (1973) Membrane properties of neuroglia in epileptogenic gliosis. Brain Res. *55:* 159–171.

Goldman, D. E. (1943) Potential, impedance and rectification in membranes. J. Gen. Physiol. *27:* 37–60.

Grossman, R. G., and T. Hampton (1968) Depolarization of cortical glial cells during electrocortical activity. Brain Res. *11:* 316–324.

Hamill, O. P., A. Marty, E. Neher, B. Sakmann, and F. J. Sigworth (1981) Improved patch-clamp techniques for high-resolution current recording from cells and cell-free membrane patches. Pflugers Arch. *391:* 85–100.

Hille, B. (1984) *Ionic Channels of Excitable Membrane*, Sinauer Associates Inc., Sunderland, MA.

Karwoski, C. J., and L. M. Proenza (1977) Relationship between Müller cell responses, a local transretinal potential and potassium flux. J. Neurophysiol. *40:* 244–259.

Karwoski, C. J., D. A. Frambach, and L. M. Proenza (1985) Laminar profile of resistivity in the frog retina. J. Neurophysiol., in press.

Kelly, J. P., and D. L. Van Essen (1974) Cell structure and function in the visual cortex of the cat. J. Physiol. (Lond.) *238:* 515–547.

Kettenmann, H., U. Sonnhof, and M. Schachner (1983) Exclusive potassium dependence of the membrane potential in cultured mouse oligodendrocytes. J. Neurosci. *3:* 500–505.

Kettenmann, H., U. Sonnhof, H. Camerer, S. Kuhlmann, R. K. Orkand, and M. Schachner (1984) Electrical properties of oligodendrocytes in culture. Pflugers Arch. *401:* 324–332.

Kimelberg, H. K. (1983) Primary astrocyte cultures—A key to astrocyte function. Cell. Mol. Neurobiol. *3:* 1–16.

Kline, R. P., H. Ripps, and J. E. Dowling (1978) The generation of b-wave currents in the skate retina. Proc. Natl. Acad. Sci. U. S. A. *75:* 5727–5731.

Kuffler, S. W. (1967) Neuroglial cells: Physiological properties and a potassium mediated effect of neuronal activity on the glial membrane potential. Proc. R. Soc. Lond. (Biol.) *168:* 1–21.

Kuffler, S. W., and D. D. Potter (1964) Glia in the leech central nervous system: Physiological properties and neuron-glia relationship. J. Neurophysiol. *27:* 290–320.

Kuffler, S. W., J. G. Nicholls, and R. K. Orkand (1966) Physiological properties of glial cells in the central nervous system of amphibia. J. Neurophysiol. *29:* 768–787.

Landis, D. M. D., and T. S. Reese (1974) Arrays of particles in freeze-fractured astrocytic membranes. J. Cell Biol. *60:* 316–320.

Landis, D. M. D., and T. S. Reese (1981) Membrane structure in mammalian astrocytes: A review of freeze-fracture studies on adult, developing, reactive and cultured astrocytes. J. Exp. Biol. *95:* 35–48.

Lothman, E. W., and G. G. Somjen (1975) Extracellular potassium activity, intracellular and extracellular potential responses in the spinal cord. J. Physiol. (Lond.) *252:* 115–136.

Miller, R. F., and J. E. Dowling (1970) Intracellular responses to the Müller (glial) cells of mudpuppy retina: Their relation to b-wave of the electroretinogram. J. Neurophysiol. *33:* 323–341.

Mori, S., W. H. Miller, and T. Tomita (1976a) Müller cell function during spreading depression in frog retina. Proc. Natl. Acad. Sci. U. S. A. *73:* 1351–1354.

Mori, S., W. H. Miller, and T. Tomita (1976b) Microelectrode study of spreading depression (SD) in frog retina—Müller cell activity and K^+ during SD. Jpn. J. Physiol. *26:* 219–233.

Newman, E. A. (1979) b-Wave currents in the frog retina. Vision Res. *19:* 227–234.

Newman, E. A. (1980) Current source-density analysis of the b-wave of frog retina. J. Neurophysiol. *43:* 1355–1366.

Newman, E. A. (1981) Regional differences in retinal Müller cell membrane properties. Soc. Neurosci. Abstr. *7:* 275.

Newman, E. A. (1984) Regional specialization of retinal glial cell membrane. Nature *309:* 155–157.

Newman, E. A., and L. L. Odette (1984) Model of electroretinogram b-wave generation: A test of the K^+ hypothesis. J. Neurophysiol. *51:* 164–182.

Newman, E. A., D. A. Frambach, and L. L. Odette (1984) Control of extracellular potassium levels by retinal glial cell K^+ siphoning. Science *225:* 1174–1175.

Nicholls, J. G., and S. W. Kuffler (1964) Extracellular space as a pathway for exchange between blood and neurons in the central nervous system of the leech: Ionic composition of glia cells and neurons. J. Neurophysiol. *27:* 645–671.

Orkand, R. K. (1977) Glial cells. In *Handbook of Physiology*. Section 1: *The Nervous System*, Vol. 1, Part 2: *Cellular Biology of Neurons*, E. R. Kandel, ed., pp. 855–875, American Physiological Society, Bethesda, MD.

Orkand, R. K., J. G. Nicholls, and S. W. Kuffler (1966) The effect of nerve impulses on the membrane potential of glial cells in the central nervous system of amphibia. J. Neurophysiol. *29:* 788–806.

Pedler, C. (1963) The fine structure of the radial fibers in the reptile retina. Exp. Eye Res. *2:* 296–303.

Ransom, B. R., and S. Goldring (1973) Ionic determinants of membrane potential of cells presumed to be glia in cerebral cortex of cat. J. Neurophysiol. *36:* 855–866.

Rasmussen, K. -E. (1975) A morphometric study of the Müller cell in rod and cone retinas with and without retinal vessels. Exp. Eye Res. *20:* 151–166.

Raviola, G. (1977) The structural basis of the blood-ocular barriers. Exp. Eye Res. *25(S):* 27–63.

Trachtenberg, M. C., and D. A. Pollen (1970) Neuroglia: Biophysical properties and physiological function. Science *167:* 1248–1252.

Trachtenberg, M. C., P. L. Kornblith, and J. Hauptli (1972) Biophysical properties of cultured human glial cells. Brain Res. *38:* 279–298.

Walz, W., and W. R. Schlue (1982) External ions and membrane potential of leech neuropile glial cells. Brain Res. *239:* 119–138.

Walz, W., W. Wuttke, and L. Hertz (1984) Astrocytes in primary culture: Membrane potential characteristics reveal exclusive potassium conductance and potassium accumulator properties. Brain Res. *292:* 367–374.

Werblin, F. S. (1978) Transmission along and between rods in the tiger salamander retina. J. Physiol. (Lond.) *280:* 449–470.

Wujek, J. R., and P. J. Reier (1984) Astrocytic membrane morphology: Differences between mammalian and amphibian astrocytes after axotomy. J. Comp. Neurol. *222:* 607–619.

Yanagida, T., and T. Tomita (1982) Local potassium concentration changes in the retina and the electroretinographic (ERG) b-wave. Brain Res. *237:* 479–483.